Engineering Structures 33 (2011) 674–684

Contents lists available at ScienceDirect

Engineering Structures

journal homepage: www.elsevier.com/locate/engstruct

Database-assisted design methodology to predict wind-induced structural behavior of a light-framed wood building

Akwasi F. Mensah [a], Peter L. Datin [a], David O. Prevatt [a,*], Rakesh Gupta [b], John W. van de Lindt [c]

[a] Department of Civil and Coastal Engineering, 365 Weil Hall, University of Florida, Gainesville, FL 32611, United States
[b] Department of Wood Science and Engineering, Oregon State University, 114 Richardson Hall, Corvallis, OR 97331, United States
[c] Department of Civil, Construction and Environmental Engineering, University of Alabama, Tuscaloosa, AL 35487, United States

ARTICLE INFO

Article history:
Received 15 August 2010
Received in revised form
1 October 2010
Accepted 16 November 2010
Available online 16 December 2010

Keywords:
Wind engineering
Wind load
Database assisted design (DAD)
Light-framed wood structure
Influence functions
Wind tunnel
Structural load paths

ABSTRACT

This study investigates the applicability of the database-assisted design (DAD) methodology to predict structural reactions in a light-framed wood structure subjected to fluctuating wind pressures. Structural influence functions were determined on a 1/3-scale light-frame wood structure, which was then subjected to a wind flow, while the surface pressures and structural reactions at roof-to-wall and wall-to-foundation connections were simultaneously recorded. There was a good agreement between the DAD-predicted structural reactions and experimentally measured reactions, confirming that the DAD method is suitable for predicting the structural reactions in light-frame wood buildings. Subsequently structural reaction time histories at several connections within the building were generated using a 1:50 scale wind tunnel model of the structure and the peak structural reactions determined using the DAD method and previously obtained influence functions. When the DAD-estimated reactions were compared with reactions predicted by the ASCE 7-05 main wind force resisting system (MWFRS) method, they showed the ASCE 7 reactions were highly non-conservative(i.e. smaller than the DAD method predictions), by as much as 39% at the gable end truss. The components and cladding method showed reasonable agreement with the DAD method for the gable end and first interior truss reactions but it too underestimated the reaction loads at the second and third interior trusses by 30% and 12% respectively.

1. Introduction

Simiu and Stathopoulos [1] proposed the use of a database-assisted design (DAD) methodology to improve wind-resistant design of buildings. The approach differs from current wind load design codified provisions that use simplified aerodynamic models supplied in reductive tables, which the authors contend can result in risk-inconsistencies. The current wind design standards, such as the ASCE 7-05 [2], includes factors such as a gust effect factor, wind load factors for hurricane and non-hurricane regions, and aerodynamic and climatological wind directional effects which have been identified to contain significant inconsistencies with regards to risk [1].

Specifically, the ASCE 7-05 [2] standard contains wind loading provisions for main wind-force resisting systems (MWFRS) that represent fictitious loading conditions that, when applied to a building, envelopes the desired structural responses (e.g. bending moments, shear, thrust) independent of wind direction (see Commentary C6.5.11 in ASCE 7-05 [2]). These provisions were developed based on results from wind tunnel tests on low-rise industrial buildings, e.g. steel portal-framed buildings, in which the measured external pressures, used in conjunction with influence coefficients for rigid frames, were spatially and time averaged to develop the maximum applied forces needed for design. The provisions result in design values that are not risk consistent, particularly when applied to other structural systems [1]. Further, the wind load standards offer no information on wind loading so that influence-function-dependent wind effects can be calculated for structural systems that differ from that assumed in the original wind tunnel tests [1].

In its present form, the wind load standard does not allow explicit consideration of spatio-temporal wind load effects and local climatological data on structural behavior. However, including such flexibility within the wind design standard is impractical because the document would become bulky with overly complex provisions.

1.1. Database-assisted design methodology

The database-assisted design (DAD) methodology was developed for use on computers in structural design offices to

* Corresponding author.
E-mail address: dprev@ce.ufl.edu (D.O. Prevatt).

0141-0296/$ – see front matter © 2010 Elsevier Ltd. All rights reserved.
doi:10.1016/j.engstruct.2010.11.028

simplify the manipulation of large databases of wind design information. The DAD methodology has three main components: (a) aerodynamic databases containing wind pressure time histories, (b) climatological databases containing historical wind speed and direction for a location, and (c) databases of structural influence coefficients to predict internal structural responses to wind loads. In the DAD framework, structural responses are numerically calculated in the following manner:

$$R_{\theta,j} = 1/2\rho V_H^2 \sum \left[N_{ij} A_i C_{p,\theta,i}\right] \quad (1)$$

where j is the reaction location; i is the pressure tap position; $R_{\theta,j}$ is the instantaneous structural response for a wind direction θ at the j-th reaction; ρ is the air density; V_H is design wind speed at building roof height; N_{ij} is the influence coefficient at the i-th pressure tap for j-th reaction; A_i is the tributary area of i-th pressure tap; and C_p is the instantaneous pressure coefficient for a wind direction θ at i-th pressure tap. With this simple approach, relying on wind-tunnel derived pressures over a building's surface and knowledge of structural load paths, reasonably accurate and risk-consistent structural reactions may be obtained.

The DAD method develops the time history of pertinent structural reactions from which the design values are determined. By knowing the influence coefficients (or influence surfaces) of specific load effects (i.e. bending moment, vertical reaction, torsion, etc.), the design wind structural responses can be determined for any component within the structure. The application of the DAD approach in practice requires software to facilitate its implementation. One example of a computer program to implement the DAD method, called *wind* PRESSURE [3], is a MATLAB-based software package for rigid, gable-roofed buildings which is in the public domain (see [4]). It uses pressure time series measured in a wind tunnel in conjunction with structural influence coefficients to compute peak values of the structural responses of interest (e.g., shear forces, bending moments, and displacements at various locations). In addition to the downloadable software from NIST, wind tunnel pressure databases for a few generic low-rise structures and influence coefficients for load effects in a steel portal framed building are also available.

A similar wind design approach, under development at the University of Notre Dame, will enable preliminary design of high-rise buildings subjected to wind loads, utilizing archives of experimental data from high frequency force balance measurements to predict overall building reactions [5].

1.2. Motivation for using DAD wind design approach

Coffman et al. [6] illustrated that simplifications in the wind design provisions of ASCE 7-05 [2] produces risk-inconsistent results for wind loading by comparing peak bending moments for steel portal framed industrial buildings calculated using the *wind* PRESSURE software and the ASCE 7-05 Analytical Method. In their study, the bending moments induced by incident winds from 36 wind directions were determined and the largest overall positive and negative moments at key locations (knee, pinch, and ridge of the portal frame) were identified. In the case of bending moment at the knee of the portal frame, Coffman et al. showed that the DAD technique yields moments that were generally 10%–40% larger than values obtained using ASCE 7-05, calculated per the main wind force resisting system. These non-conservative values provided by the ASCE 7-05 analysis occurred consistently in other locations, while the extent of under-estimation varied widely (from 15% to 70%). Despite the proposition that DAD predicts wind design loads on low rise buildings with better accuracy than current design standards, its application has been limited because wind pressure databases are not available for many building geometries and the influence functions, particularly for wood-framed buildings, are generally unknown.

There has been growing interest in understanding the structural load paths in light-frame wood structural systems. Several researchers have conducted full-scale experiments [7–9], scale model experiments, and analytical studies to understand wind load paths [10–12].

1.3. Objective of the study

The purpose of this study is to evaluate the applicability of the DAD approach for wind design of light-frame wood structures (LFWS). Structural influence coefficients (surfaces) were experimentally determined on a 1/3-scale wood-framed model of a gable-roof building. To validate the DAD approach for LFWS, the model building was subjected to a wind flow while simultaneously measuring pressures on the roof and wall and structural reactions at critical locations. Structural reactions were predicted using the measured wind pressures and the influence coefficients via a DAD-based MATLAB program and compared to the directly measured reactions. Furthermore, wind pressure time series on a 1/50-scale model of the prototype building were determined in an atmospheric boundary layer wind tunnel for five wind azimuths and used to predict structural reactions. DAD-based predictions were compared to structural reactions estimated based on ASCE 7-05 provisions. A flowchart of the components of the study is presented in Fig. 1. This research is part of a three-university collaborative study to better understand structural load paths in light-framed wood structural (LFWS) buildings, with the overarching goal to develop a performance-based design methodology for wind-loading on light-frame wood structural systems [13].

2. Experimental validation of DAD method for a LFWS system

2.1. Wood house/instrumentation

A 1/3 scale wood structure was built to represent a prototype structure with a rectangular floor plan of 12.2 m by 9.2 m (40 ft by 30 ft), ridge height of 4.2 m (13.8 ft), a 4 in 12 sloped-gable roof, and roof eaves extending 0.45 m (18 in.) beyond the exterior walls. The model framing member sizes were established using non-dimensional geometric scaling laws [14,15], with cross-sections of 12.7 mm by 29.7 mm (0.5 in. by 1.17 in.) representing a typical nominal 2 × 4 framing member. The structure was built using typical materials used in residential construction in the southeastern United States: southern yellow pine for roof trusses and spruce-pine-fir for wall studs. The roof and wall sheathing used on the model was 6.4 mm (0.25 in.) oriented strand board, scaled to represent the 12.7 mm (0.5 in.) thick OSB used at full scale. The walls have external sheathing only with no window or door openings. Typical spacing of the model scale roof trusses was 200 mm (8 in.) o.c. and the wall studs were spaced at 133 mm (5.3 in.) o.c. The building model (Fig. 2) has a rectangular floor plan measuring 3 m (10 ft) wide by 4.1 m (13.3 ft) long and a ridge height of 1.4 m (4.6 ft).

Twenty-one ±1300 N (300 lb) capacity uniaxial load cells were installed in the model house at critical locations: twelve at roof-to-wall connections and nine at the wall-to-foundation connections (Fig. 3(a)). Twenty-nine pressure taps were also installed: twenty-five distributed on the roof near the gable end and four installed in the walls — two in the side wall and two in the gable end wall (Fig. 3(b)). The pressure taps were connected to differential transducers (± 6.9 kPa or ±1 psi) via 152.4 mm (6 in.) long, 4.8 mm (0.19 in.) inside diameter (ID) vinyl tubing. The load cells were connected to signal conditioners and signal amplifiers to increase the accuracy of the readings. After passing through the signal amplifiers, a data acquisition unit recorded the signals using a laptop connected via USB running a National Instruments LabVIEW data acquisition program.

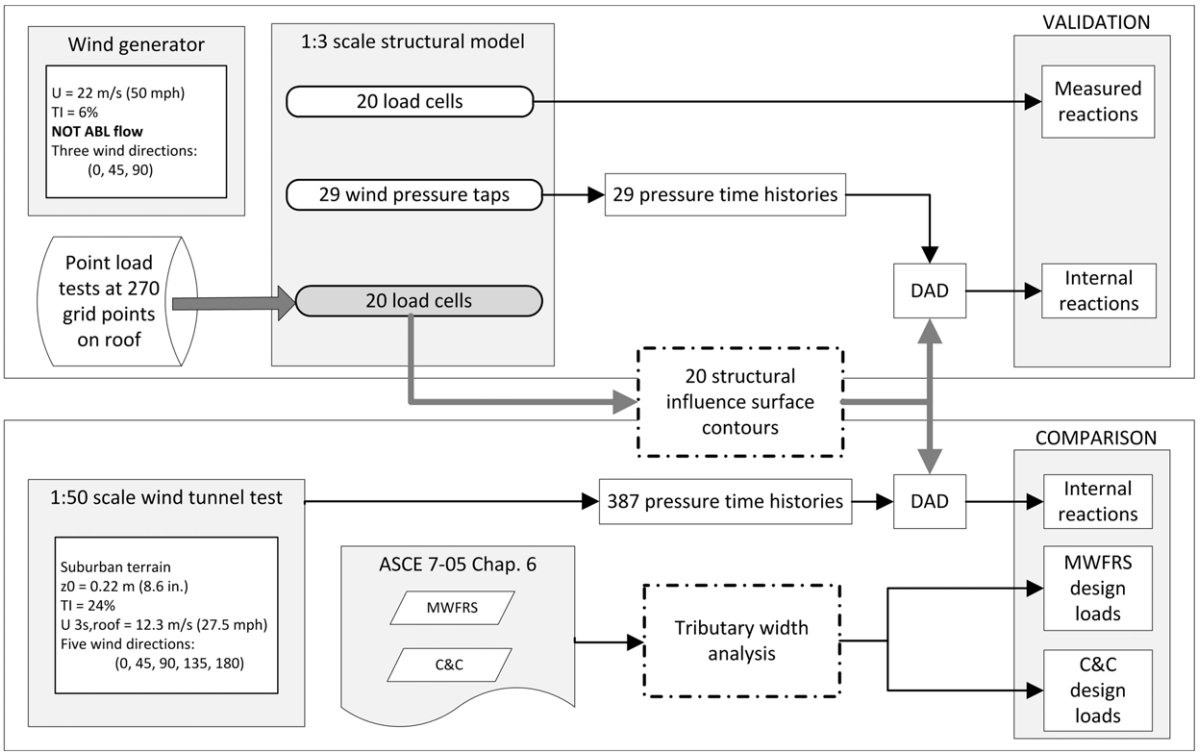

Fig. 1. Research flowchart (Note: MWFRS denotes main wind force resisting system and C&C denotes components and cladding).

Fig. 2. 1/3-scale light-framed wood model building used in the study (wall pressure taps w1 and w2 are clearly seen on side wall).

2.2. Structural influence functions

The influence coefficients for vertical uplift reactions were experimentally determined on the 1/3 scale building. A grid of 270 load application points distributed over the roof surface was used to apply upward and downward loads perpendicular to the roof surface. For each point load application the structural reactions were monitored at all instrumented connections. The influence coefficient, N_{ij} for the i-th load application point (at the j-th reaction location) was calculated as the load at the j-th reaction location divided by the applied load, thus representing the percentage of the applied force transferred through the j-th connection.

In the study, two roof structural attachment arrangements along the gable end wall were considered and influence functions determined in each case. Influence functions were derived twice for Case 2 as noted below.

Case 1: Three intermediate connection points (S1, S2 and S3) were installed along the bottom chord of the gable end truss attaching the truss to the wall.

Case 2a: The three intermediate connection points (S1, S2 and S3) along the bottom chord of the gable end truss were removed. This test was done in November 2009.

Case 2b: The three intermediate connection points (S1, S2 and S3) along the bottom chord of the gable end truss were removed. This test was done in May 2010 following the wind generator test performed in March 2010.

The structural configurations and influence surfaces developed in Case 1 and Case 2a were used for the DAD analysis with wind tunnel data. As explained later in the paper, the influence surfaces developed for structural configuration Case 2b, were used to experimentally validate the DAD methodology in the wind generator tests.

2.3. Wind generator test arrangements and procedure

A wind generator was used to create wind flow around the 1/3-scale building during which pressure variations on the roof and structural reactions at critical locations were monitored. The wind generator consists of an 8-fan array of 1.4 m (4.5 ft) diameter, vane–axial fans, hydraulically powered by four 700 hp marine diesel engines [16]. The fans channel air through a contraction area leading to a 3 m by 3 m (10 ft by 10 ft) exit. The generator was designed primarily for testing window and door panels [16] and does not re-create hurricane wind fluctuations or atmospheric boundary layer flow. The 1/3-scale building was placed between two 4.9 m (16 ft) tall walls 5.5 m (18 ft) downstream of the generator exit (Fig. 4). A mean wind speed of 22 m/s (50 mph) with a turbulence intensity of 6% was used in the experiment. A 4-hole Cobra Probe (Serial #193), by Turbulent Flow Instrumentation, Inc., was used to verify the uniformity downwind of the contraction exit (with no model in place) with a sampling frequency of 10,000 Hz.

The model building was oriented for wind flow in three angles of attack — 0°, 45°, and 90° — with three 10 min duration test runs each. Pressure and load measurements were simultaneously taken at a sampling rate of 200 Hz and low-pass filtered at 100 Hz. The

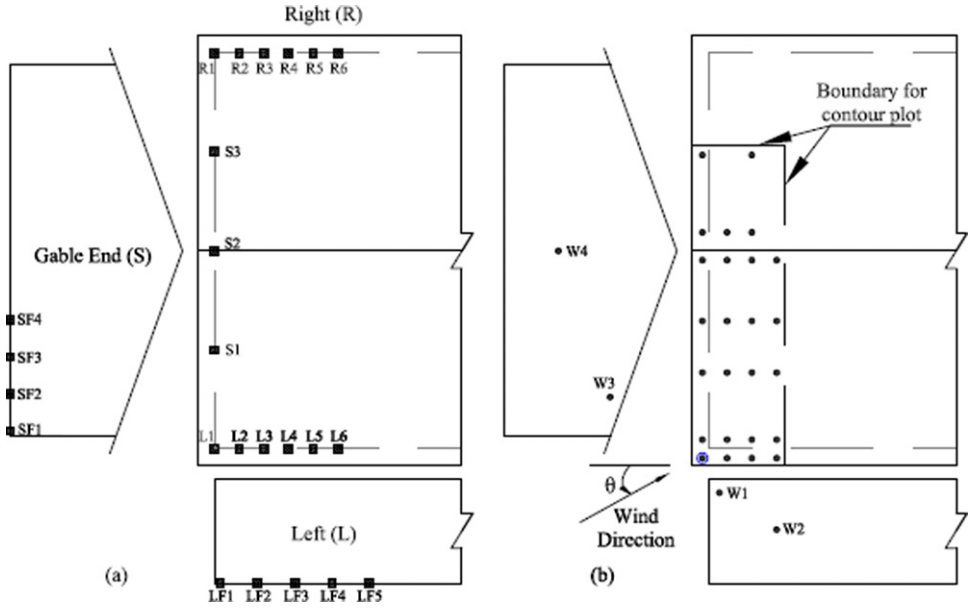

Fig. 3. Plan and elevations showing locations of load cells (square symbols) and pressure taps (circles) on the model building. (Note: the soffit pressures for corner pressure tap location (circled tap) is averaged from the wall pressures on the side and gable end walls).

Fig. 4. 1/3-scale model building, wind generator prior to validation testing. (Model was tied down to minimize buffeting).

wind velocity at the mean roof height and upwind of the model building was measured using the Cobra Probe.

3. Results

3.1. Influence surfaces

The influence surfaces obtained for roof-to-wall reactions are shown in Fig. 5. The influence coefficients for the gable truss reaction connections when the truss does not have intermediate connections (Case 2a) are higher than those obtained in Case 1 (where intermediate connections are provided) as seen in Fig. 5(a). In Fig. 5(b), the influence surfaces at R2 are essentially symmetrical with L2. As a result, we mirrored the influence surfaces from the left side (L1 through L6) in our analysis to the right side roof-to-wall connections (R1 through R6). It may be observed also in Fig. 5(c) that similar influence surfaces were obtained at interior roof-to-wall connections.

Fig. 6 shows the influence surfaces for vertical reactions at several wall-to-foundation connections. The peak influence coefficient in this case was 0.35, for SF1. The influence surfaces obtained at reactions LF3, LF4, LF5 and SF4 were similar to that for SF3 (Fig. 6(b)). For the wall-to-foundation connections, the influence coefficients were also uniformly distributed over the roof area, suggesting that the sheathed wall behaves like a deep beam on a uniform support with sufficient load paths for loads to spread away from point of application.

3.2. Influence functions: Case 2a vs. Case 2b

The influence surfaces developed for Case 2a and Case 2b configurations were essentially similar for all connections except the gable end truss connections, L1 and R1. To illustrate the differences, Fig. 7(a) and (b) present the influence coefficients for connections L1 and L2 when a moving point load is applied directly along the gable end and first interior trusses, respectively. Fig. 7(c) shows the influence coefficients for L2 when the load was applied along the gable end truss. The influence coefficients for L1 are reduced in Case 2b as compared with the Case 2a earlier configuration by as much as 0.2 at R1 (Fig. 7(a)), there is insignificant change between influence lines for L2. However, Fig. 7(c) shows a relatively large increase in influence coefficients at L2 in Case 2b when the load is applied to the gable-end truss. This behavior occurred during three repeats of the Case 2b influence function tests for these connection locations, and similar results were observed for the gable end and first interior truss connections on the opposite side wall.

The results strongly suggest that inadvertent displacement of the gable end truss occurred during transportation of the model house to the wind generator test location. The displacement may have reduced the vertical stiffness of the gable end truss connections causing it to shed load, sharing a larger proportion to the adjacent (stiffer) connections. The negative influence coefficients observed in Case 2b are indicative of rigid body rotation of the stiff gable truss (relative to the wall plate support), resulting in a net downward reaction at L1 (and R1).

The authors acknowledge that while Case 2a influence surfaces are representative of the expected structural configuration for this building type, the Case 2b influence surfaces (see Fig. 8) were used for validation of the DAD methodology using the wind generator because it best represented the actual structural configuration in existence at the time of the tests.

3.3. Experimental measurements and DAD estimates

Contour plots of peak pressure coefficients on the building roof from testing with the wind generator are shown in Fig. 9. Wind

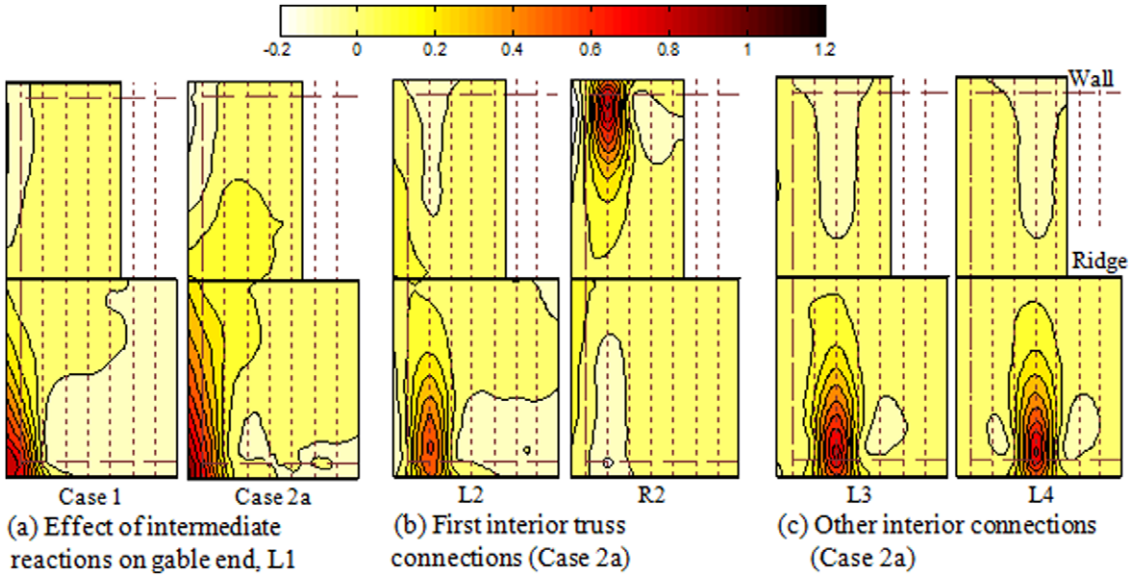

Fig. 5. Typical influence surface contours for vertical reaction at roof-to-wall connections.

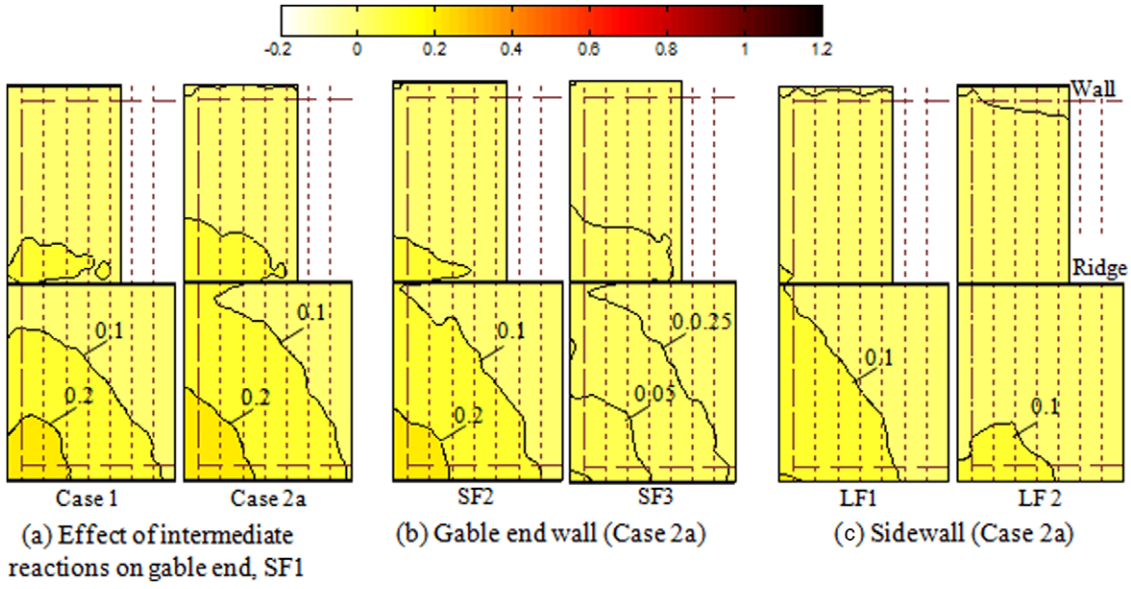

Fig. 6. Typical influence surface contours for vertical reactions at wall-to-foundation connections.

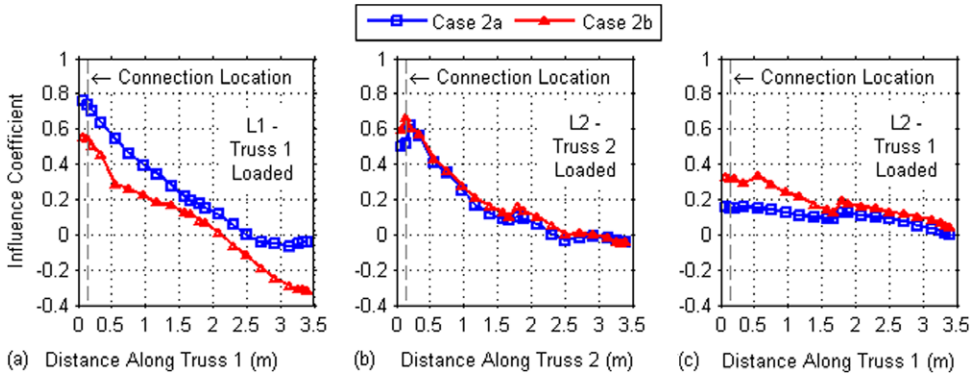

Fig. 7. Influence lines along trusses 1 and 2 measured at L1 and L2 before and after the wind generator test.

pressures were normalized by the wind velocity measured by the Cobra Probe at the mean roof height. The wind distribution over the roof of the building was generally characterized by peak suctions especially for the 0° and 45° azimuths. High suctions were recorded along the gable edge of the roof while relatively low suctions were measured at the interior roof areas of the roof for the 45° azimuth.

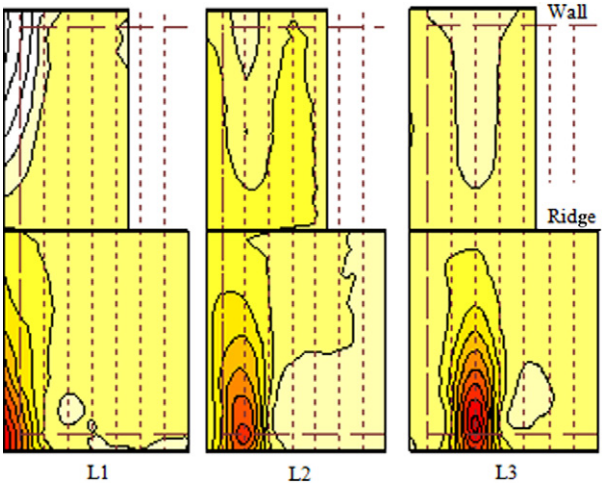

Fig. 8. Influence surface contours from the May 2010 experiment used in the DAD validation test.

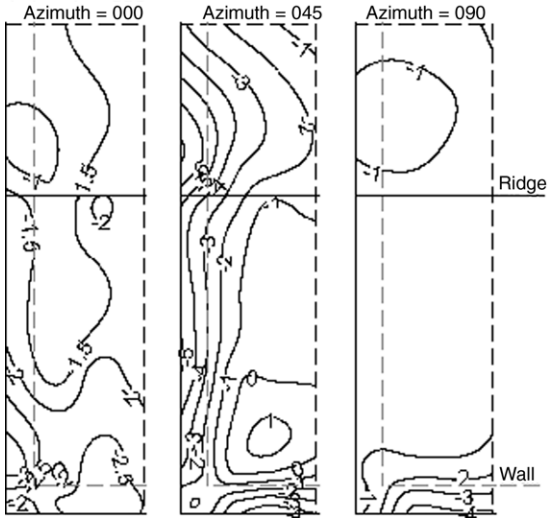

Fig. 9. Contours of peak negative pressure coefficients on the roof.

For the 90° azimuth however, relatively low suctions enveloped the roof of the house except at the eave-end area. The spatial variations obtained on the 1/3-scale building are in reasonable agreement with wind tunnel pressure distributions (shown later in Fig. 17).

The time series of wall pressure coefficients at w1 and w3 (in Fig. 3) are assumed to be representative of the uniform pressure distributed along the bottom surface of the eave overhang. They were therefore added to the roof pressure coefficient time series at pressure taps along the overhang regions to account for soffit pressures. This was based on a finding that soffit pressures are nearly fully correlated with nearby wall pressures with excellent agreement (average of 7% difference) between their peak negative values [17]. Fig. 10 shows contour plots of peak coefficients of total roof pressures, including eave pressures.

Structural reactions at the connections L1, L2 and L3 were estimated by numerically combining the wind pressure time histories using two methods: (1) roof pressures only and (2) using the total pressure on the roof (from upper and lower soffit surfaces on overhang roof areas), with experimentally derived influence coefficients (Case 2b) in a DAD framework.

Fig. 11 shows the power spectral density (PSD) plots (typical) of the structural reactions measured and estimated using the DAD methodology. The DAD estimated PSDs were determined for total

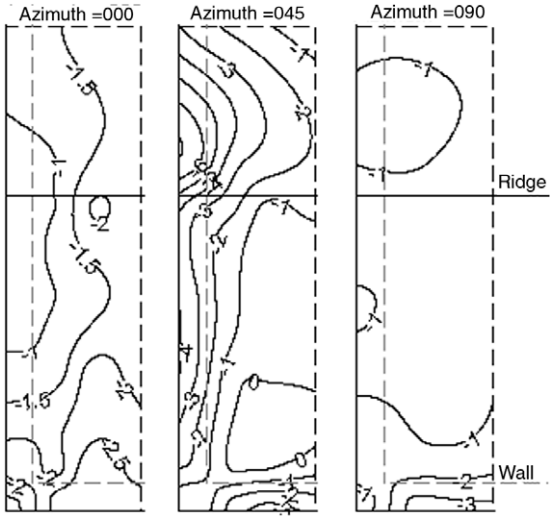

Fig. 10. Contours of peak negative pressure coefficients on the roof with added overhang pressures.

pressure on the roof including roof surface and soffit pressures. As expected, most of the energy falls within low frequencies (0–5 Hz). There is also a good agreement between the PSDs of measured and estimated reactions. The spike observed in the estimated reactions (at frequency of 55 Hz) could be attributed to the tubing system used in the experiment and/or limitation of the pressure transducers to accurately capture energies at high frequencies since the spike was not seen in the PSDs of the wind flow nor the measured reactions. A cut-off frequency of 5 Hz was selected and the data low-pass filtered (using an eighth-order Butterworth filter) to generate the reaction time histories.

Fig. 12 shows the first 60 s time histories of experimentally measured reactions compared to DAD-estimated reactions using only the roof pressures for L1 for wind azimuths 0° and 45°. Without, the inclusion of soffit pressures, DAD consistently underestimated the measured reactions. However, there is generally a good agreement between the measured structural loads and reactions estimated when the soffit pressures are included (as seen in Fig. 13). A correlation coefficient of 0.9 was measured between the time histories in Fig. 13. The expected peaks, means and standard deviations of the measured and estimated reactions using the total pressures at connections L1, L2 and L3 are presented in Table 1. There is reasonable agreement between the statistical values of measured and estimated (total) reactions, especially for the gable end and first interior connections, L1 and L2 respectively. There is less agreement for the L3 connection because the limited distribution of the pressure taps did not completely cover the area of influence of the L3 connection. In addition, the discrepancy between the measured and estimated reactions could be that the course geometric layout of the pressure taps provides insufficient resolution to capture the spatial pressure distribution. Also, simplifying assumptions were made regarding the temporal variation and magnitude of the overhang pressures using two wall pressure taps (one per each side).

Table 1 also includes results comparing the measured and estimated reactions when the model building was oriented at 90° to the wind. In all three cases there was poor agreement between measured and estimated reactions, both for peak and mean loads. This was somewhat expected due to the limitations in the experimental setup that prevented the wind flow from completely enveloping the structure, thus resulting in unnatural results.

With the comparison of the DAD-based and directly measured reactions showing sound agreement, it can be concluded that the DAD approach can predict structural reactions with reasonable

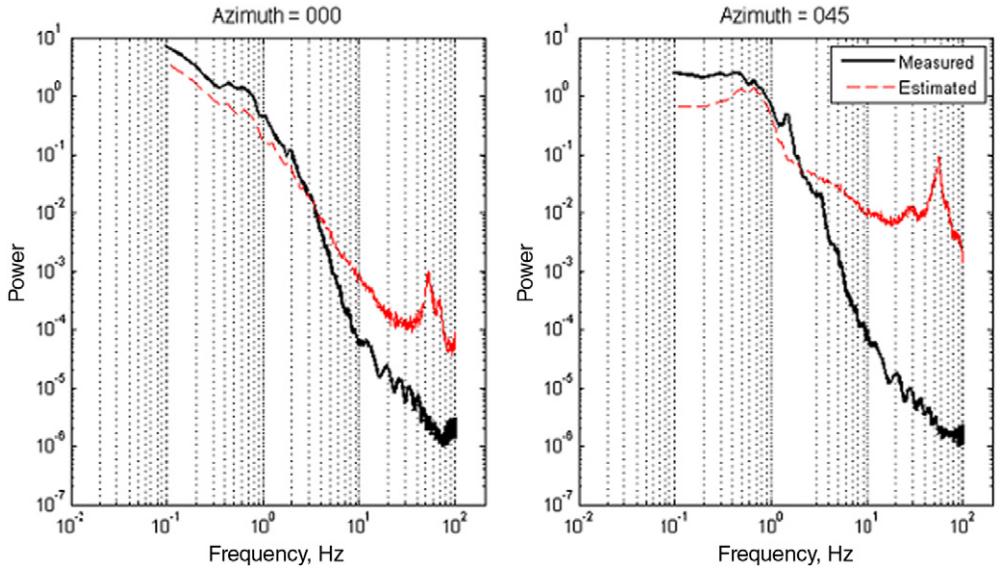

Fig. 11. Power spectra of DAD estimated and measured vertical reactions at L1 connection.

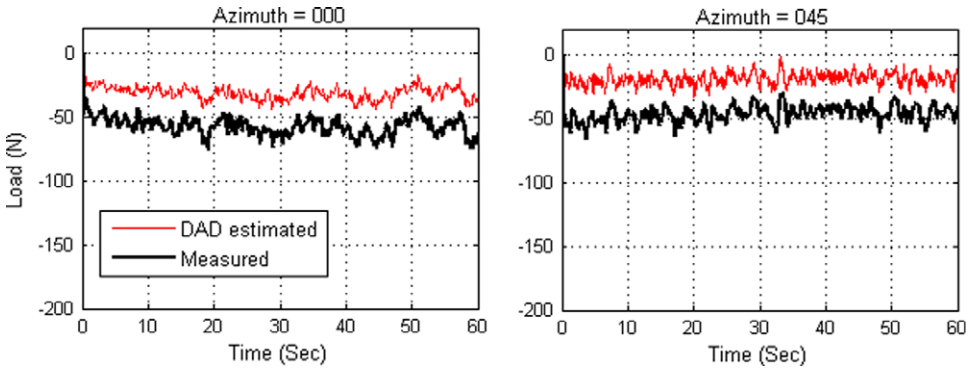

Fig. 12. 60 s time histories of vertical reaction estimated by DAD method for L1 connection (thicker line is measured load).

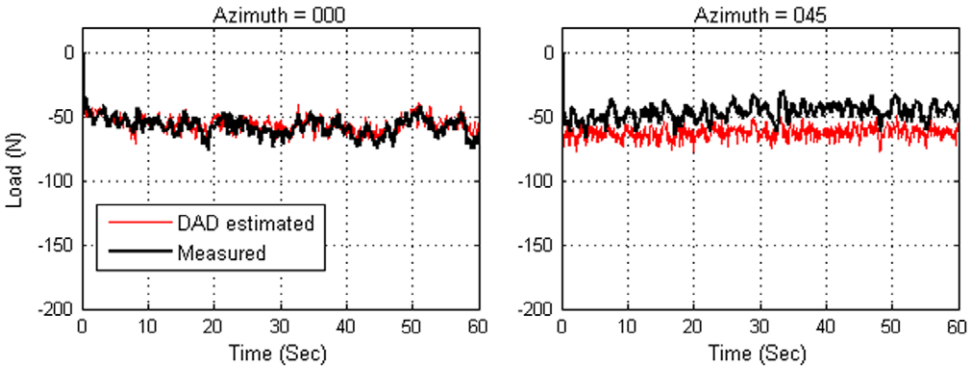

Fig. 13. 60 s time histories of total vertical reaction by DAD method for L1 connection (including soffit pressures). Note measured load (thicker line) is the same as in Fig. 11.

accuracy. The next section looks at estimating structural reactions using more realistic pressure distributions from a wind tunnel study.

4. Wind tunnel study

4.1. Boundary layer wind tunnel and instrumentation

Wind tunnel studies were conducted on a 1:50 scale model in Clemson University's boundary layer wind tunnel, which is an open-return wind tunnel with an 18 m (60 ft) long by 3 m (10 ft) wide by 2.1 m (6.9 ft) tall test section and is powered by two 1.8 m (6 ft) diameter fans. Test models are mounted on a 2.7 m (9 ft) diameter turntable, approximately 15 m (50 ft) from the test section entrance. A detailed description of the wind tunnel setup and instrumentation are described in [18], but pertinent highlights are provided below.

A suburban wind velocity profile (Fig. 14) was simulated in the tunnel having a full-scale roughness length zo of 0.22 m (0.72 ft) and a longitudinal turbulence intensity of 24% at mean roof height of the model. The wind speed at the reference height in the tunnel — 300 mm (12 in.) below the tunnel ceiling — was approximately 13 m/s (29 mph).

Table 1
Comparison of peak and mean values of DAD-estimated and measured reactions at L1, L2 and L3 connections from 1/3-scale model building validation tests (in Newtons).

	Reactions	L1			L2			L3		
		Peak	Mean	St. dev.	Peak	Mean	St. dev.	Peak	Mean	St. dev.
0°	Measured	−101.8	−68.1	10.6	−87.8	−70.1	6.6	−113.8	−82.8	10.1
	Estimated	−87.6	−57.5	8.2	−98.8	−63.9	10.1	−78.1	−47.5	8.2
45°	Measured	−77.9	−53.8	7.0	−58.2	−44.0	3.8	−71.7	55.7	4.7
	Estimated	−88.8	−67.8	4.9	−103.4	−76.1	6.8	−66.9	−47.8	5.2
90°	Measured	−14.9	8.4	6.8	−72.3	−40.7	6.6	−10.8	6.0	4.4
	Estimated	−48.8	−8.7	10.5	−55.0	−12.8	10.6	−38.7	−8.5	7.9

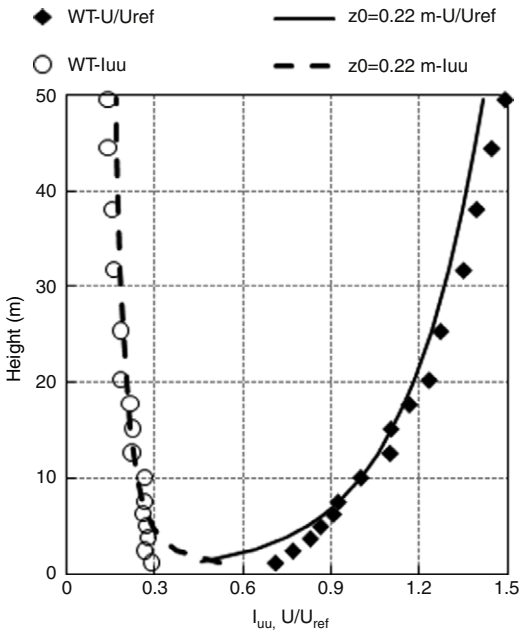

Fig. 14. Mean wind speed and turbulence intensity profiles for suburban exposure in wind tunnel. (Note: Uref is mean wind speed at 10 m (full-scale); WT is wind tunnel data; Iuu is longitudinal turbulence intensity).

Fig. 15. 1:50 scale model building used in wind tunnel study.

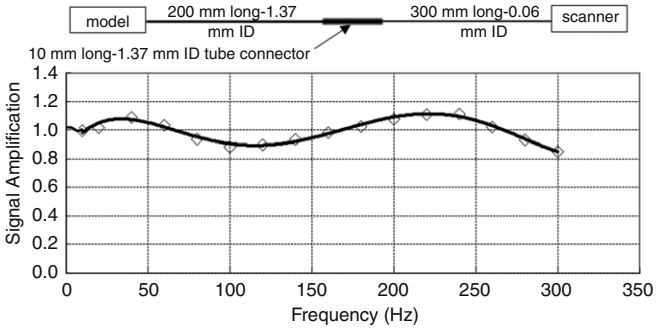

Fig. 16. Frequency response of tubing and arrangement of pressure tubing system.

4.2. Scale model and pressure measurements

387 pressure taps were installed in the roof of the 1/50-scale model, which was 366 mm (14.4 in.) long by 183 mm wide (7.2 in.) in plan (Fig. 15). The pressure taps were made of metal tubes with an outside diameter of 1.6 mm (0.063 in.) glued to acrylic sheets. Near simultaneous pressure time-histories were recorded using six Scanivalve ZOC33 electronic pressure scanning modules, which were connected to a RAD3200 digital remote analog to digital converter. Pressure taps from the building model were connected to the measuring system using a 300 mm (12 in.) long tubing system with a frequency response shown in Fig. 16. Wind tunnel tests were performed at five wind directions (0°, 45°, 90°, 135° and 180°) with eight repeats per azimuth. Pressure data was sampled at 300 Hz for 120 s and then low-pass filtered at 150 Hz and corrected for tubing response.

4.3. Pressure coefficients

The pressure coefficients $C_{p,\mathrm{ref}}$ were determined as:

$$C_{p,\mathrm{ref},i} = \frac{P_i}{1/2\rho U_{\mathrm{ref}}^2} \tag{2}$$

where the pressure coefficient $C_{p,\mathrm{ref}}$ is the ratio of tap pressure P_i divided by the mean dynamic pressure recorded by a pitot tube at a reference height located 300 mm (12 in.) below the wind tunnel ceiling directly above the model, ρ is the air density, and U_{ref} is the mean wind velocity at the reference height.

Aerodynamic data referenced to mean roof height dynamic pressure produces the least variability [19], hence the pressure coefficients were normalized to a 3 s gust wind speed at mean roof height, $U_{3s,h}$. An adjustment factor C_a, defined in Eq. (3), was used to convert the wind tunnel pressure coefficients $C_{p,\mathrm{ref}}$ to the equivalent coefficient $C_{p,h}$ referenced to the 3 s gust wind speed at mean roof height, h. The wind speeds were taken from the velocity profile. The 3 s gust wind speed at mean roof height $U_{3s,h}$ was 12.3 m/s (27.5 mph), and the mean reference wind speed U_{ref} was 13 m/s (29 mph).

$$C_{p,h} = C_a \cdot C_{p,\mathrm{ref}} = \left(\frac{U_{\mathrm{ref}}^2}{U_{3s,h}^2}\right) \cdot C_{p,\mathrm{ref}}. \tag{3}$$

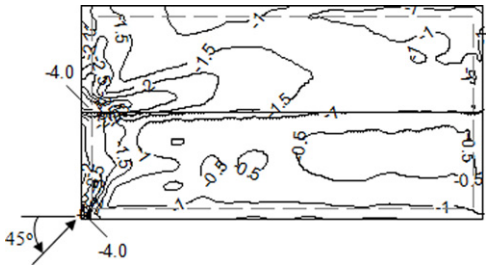

Fig. 17. Distribution of expected peak negative pressure coefficients on wind tunnel model for 45° wind azimuth.

The Lieblein–BLUE (Best Linear Unbiased Estimator) fitted extreme pressure coefficient contour plots for the 45° wind direction are presented in Fig. 17. Details of the BLUE estimation [20] of expected peaks from the eight measured individual peaks of each tap can be found in [21].

5. Applying the DAD methodology using wind tunnel derived pressure database

5.1. Prediction of structural reactions

Structural reactions at each of the instrumented connections were estimated based on the DAD approach using the wind tunnel pressure coefficients and the structural influence surfaces along with a single velocity pressure computed from ASCE 7-05 [2]. Instantaneous reaction time histories at each location were computed using Eq. (1). A velocity exposure coefficient of 0.70 (Table 6.3 in ASCE 7-05) was used to transform a 3-s gust design wind speed of 58 m/s (130 mph) over open terrain to an equivalent design wind speed at a mean roof height of 4.2 m (13.8 ft) in a suburban exposure. Eight sample mean and peak values were measured from the reaction time histories obtained for each wind direction.

5.2. Probability density functions and expected peaks

Fig. 18 shows representative histograms for predicted roof-to-wall and wall-to-foundation reactions using the wind tunnel pressures. The best fit to the reactions is a reverse 3-parameter lognormal distribution, which is the lognormal distribution mirrored about the vertical axis allowing the longer tail to trail to the left. The probability density function, $p(x)$, of the 3-parameter lognormal distribution is given by:

$$p(x) = \frac{1}{(x-\theta)\,\sigma\sqrt{2\pi}} \exp\left[-\frac{1}{2}\left(\frac{\ln(x-\theta)-\mu}{\sigma}\right)^2\right] \qquad (4)$$

where θ is the location parameter, μ is the scale parameter, and σ is the shape parameter. Values of these parameters used in generating the distributions are provided in Fig. 18.

Fig. 18 shows a significantly larger spread of reactions obtained for the 0° wind azimuth and reduces with increasing angle of incident wind at the gable end reaction (L1). This is likely due to the high spatial and temporal fluctuations in wind pressure distribution near the reaction for the smaller wind angles (e.g. 0° and 45°). The reaction time histories at this location therefore contain higher fluctuating components for these wind azimuths.

Expected peak reactions were estimated from the eight extreme values for each wind direction using the Lieblein–BLUE method [20]. The validity of using the extreme value Type I distribution for the peaks was confirmed by using the Anderson–Darling goodness-of-fit test [22]. Using the distribution parameters estimated from the Lieblein–BLUE method, 95% of the peak reaction distributions fit the extreme value Type I distribution well (p-values > 0.25).

The expected peak and mean reactions for the wind azimuths are presented in Figs. 19 and 20. The highest load occurs at the gable end and structural loads reduce at successive interior connections. In Case 1 (Fig. 19), the peak wall-to-foundation loads occurring at SF2 is significantly higher than the peak roof-to-wall connection loads directly above it at S1 and L1 for 0° and 45° wind azimuths. It is interesting to note that the peak wall to foundation reaction occurs not at the corner but approximately 1.5 m (4.8 ft) away along the gable-end wall, when the bottom chord of the gable end truss is connected to the wall. However, in Case 2 (Fig. 20), the gable end corner reaction (SF1) has the largest load for the foundation connections with the gable end roof-to-wall connections (L1 and R1) experiencing even higher loads.

As shown in Figs. 19 and 20, the critical (peak-enveloped) reactions at most of the roof-to-wall connections and all the wall-to-foundation are observed at wind direction 0°. For Case 1 (with intermediate connections on the gable-end truss), as much as 17.51 kN (3935 lbs) of load is transferred through the three intermediate connections (S1, S2, S3) while truss end connections (L1 and L2) carry a total load of 9.2 kN (2066 lbs). However in Case 2 when the intermediate connections are removed, the total load carried by L1 and L2 increased by 67% (6.13 kN (1378 lbs)). In Case 2, the remaining 33% of the load from intermediate connections is shared among the other interior truss connections. At the wall-to-foundation connections, there were marginal differences between reactions for the two cases. In both cases also, the connections SF1 and SF2, nearest to the gable end wall corner experienced the highest load transfers at the foundation level. A similar observation is made at the side wall foundation connections where higher loads are observed at connections LF1 and LF2 but reduce drastically at the other interior connections.

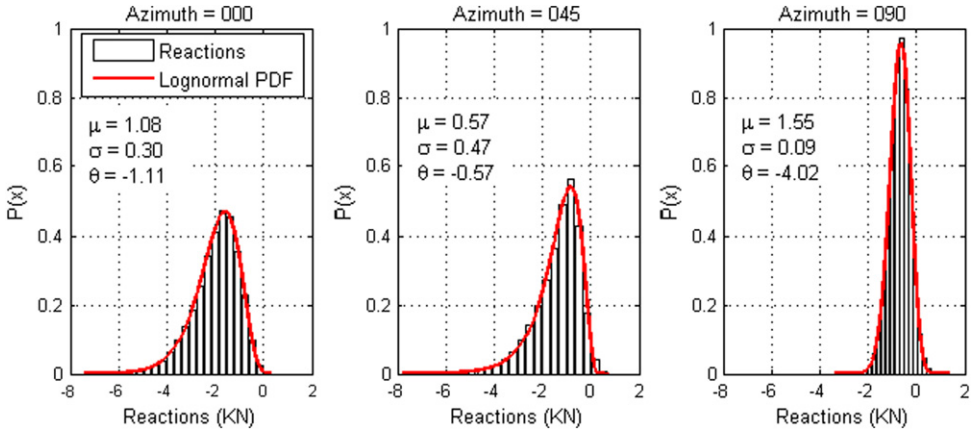

Fig. 18. Probability density functions of reactions at L1 connection.

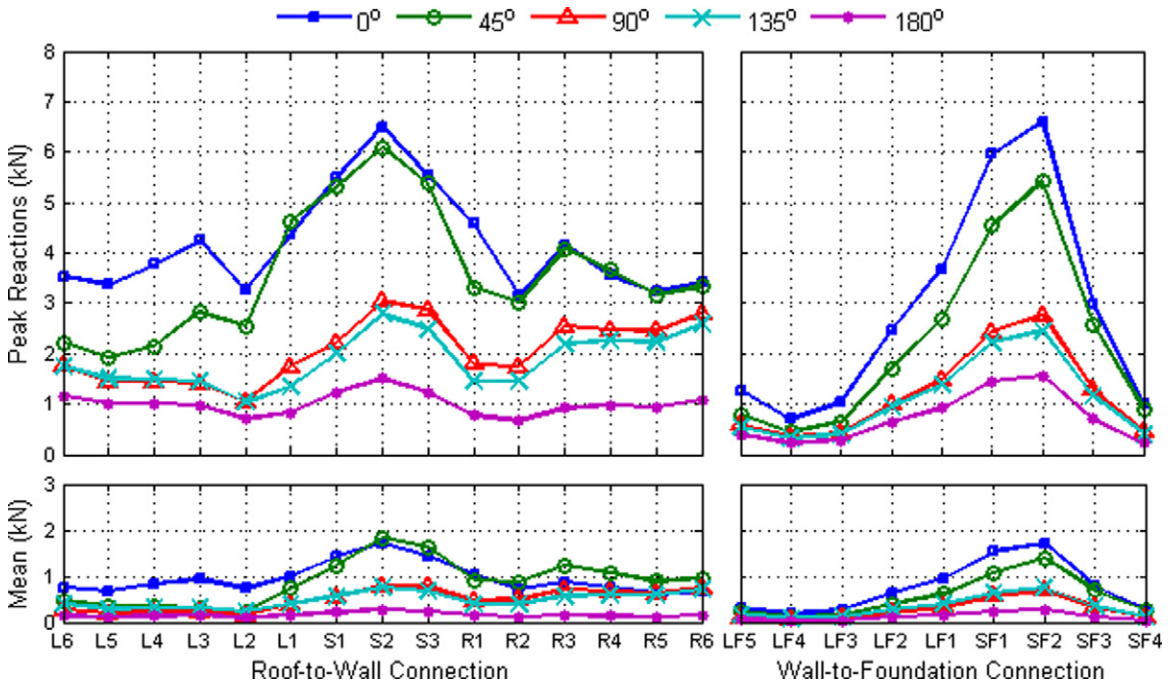

Fig. 19. Expected peak negative and mean vertical reactions Case 1, (with intermediate connections along bottom chord of gable-end truss).

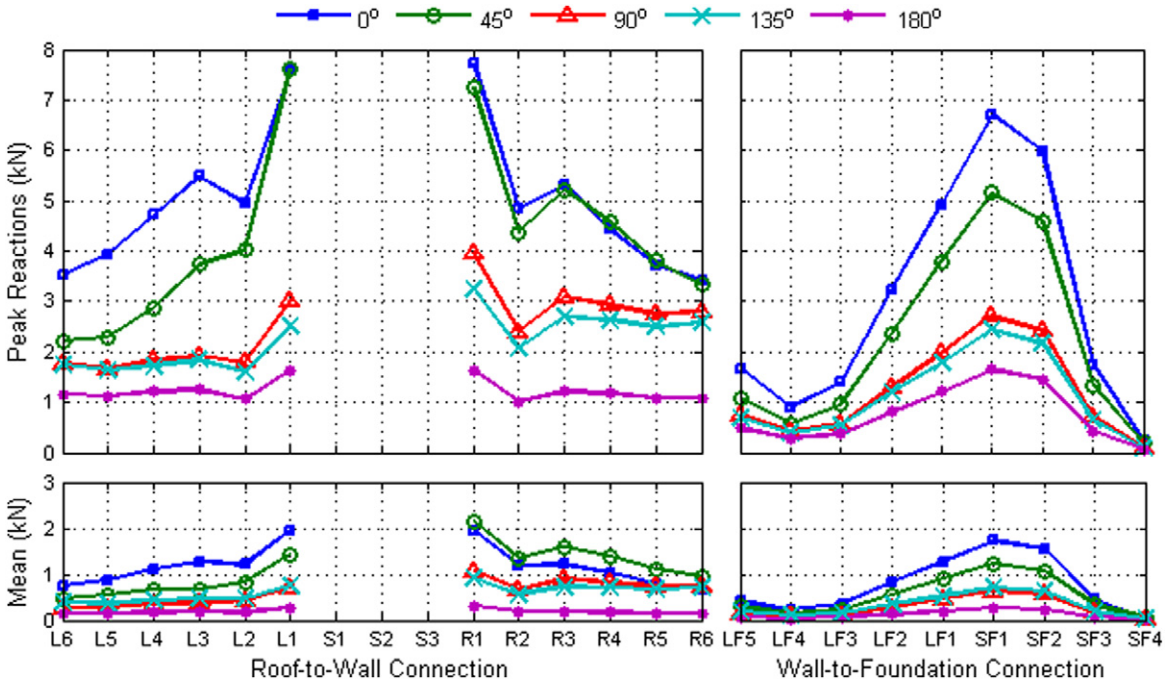

Fig. 20. Expected peak negative and mean vertical reactions Case 2, (without intermediate connections along bottom chord of gable-end truss).

6. Comparison of DAD predicted reactions versus ASCE 7-05 wind loads

In comparing the DAD results with ASCE 7-05, no internal or overhang pressures were considered in either the DAD or ASCE 7 estimations. The wind design loads were determined assuming a wind directionality factor, K_d, of 0.85, with the importance factor, I, and the topographical effect factor K_{zt} taken as unity in all cases. The DAD-predicted reactions were compared with both the Main Wind Force Resisting System (MWFRS) and the Components and Cladding (C&C) design loads. Design pressures for MWFRS of the low-rise building were determined based on Eqs. (6)–(18) and Figs. 6–10 of the ASCE 7 [2]. The components and cladding wind pressures were determined using Eqs. (6)–(22) and Figs. 6–11C with an effective wind area of 300 ft^2 (determined as the product of the span, (30 ft), by one-third of the span length).

Structural reactions at roof truss-to-wall connections predicted by ASCE 7-05 and the DAD method are compared in Fig. 21. For the gable end truss, the DAD-estimated peak reaction is 39% higher than that predicted by the MWFRS procedure. The MWFRS underestimates the DAD-based reactions at the first three interior trusses by 14%, 26% and 18% respectively. The results showed better agreement between the DAD and MWFRS methods at the fourth and fifth interior trusses, although this could also be due

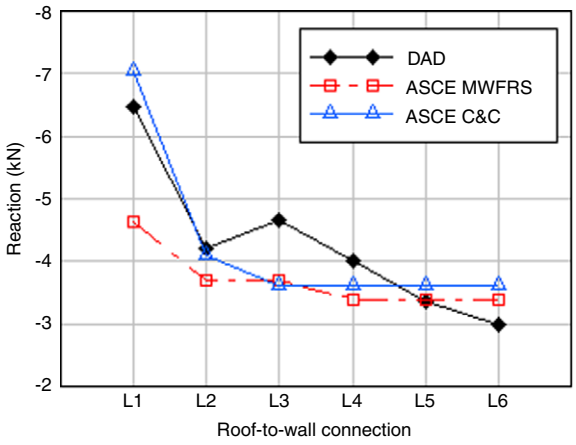

Fig. 21. Comparison of DAD and ASCE 7-05 estimated structural reactions at roof-to-wall connections.

to experimental limitations, since the influence surfaces may not have extended sufficiently to completely capture the load transfers.

The ASCE 7-05 components and cladding (C&C) method showed reasonable agreement with the DAD method for the gable end and first interior truss reactions (with 8% and 2% differences respectively), but it too underestimated the reaction loads at the second and third interior trusses by 30% and 12%, respectively. The C&C method appears to be conservative at the fourth and fifth interior trusses, predicting reactions that are 7% and 16% higher than DAD-estimated reactions. It should be noted that if additional wind directions (i.e. azimuths producing cornering vortices) were used in the DAD analysis, the percentage differences could only increase, since the critical reaction would be produced by the enveloped maxima which may not have been captured by one of the five wind azimuths considered in this study.

7. Conclusion

This paper presented the background, methodology and results to validate and utilize the database assisted design methodology for predicting the structural reactions in a light-frame wood residential building. A background to the DAD methodology was presented and its applicability to wind design of low-rise, wood-framed structures identified. An instrumented 1/3-scale light-frame wood model building was used to determine structural influence surfaces and to conduct a wind flow experiment. The DAD methodology predicted the structural reactions at the roof-to wall and wall-to-foundation connections using wind pressures measured on the model and the structural influence surfaces. There was good agreement between the DAD-predicted reactions and directly measured loads. The results showed that the DAD methodology is suitable for predicting structural loads in wood-framed structures.

The peak structural reactions predicted using the DAD method were consistently greater than the peak structural reactions predicted by ASCE 7-05, for four trusses nearest to the gable end. The ASCE 7-05 main wind force resisting system (MWFRS) method predicted highly non-conservative roof-to-wall reactions that were as much as 39% lower than the DAD-estimated reactions for the gable end truss. While the reactions predicted by the components and cladding method were in reasonable agreement for the gable end and first interior truss, it still underestimated the reaction loads at the second and third interior trusses. Experimental limitations in this study (i.e. extent of developed influence surfaces, and limited number of wind azimuths) suggest that the actual level of non-conservatism in the ASCE 7-05 values could only increase (i.e. the DAD reactions are likely to increase), if additional wind azimuths and a larger influence surface coverage were used on the roof of the model building.

Acknowledgements

This material is based upon work supported by the National Science Foundation under Grant No. 0800023 and the authors gratefully acknowledge their financial support. In addition, the authors are appreciative for access to and operation of the wind generator provided by Dr. Forrest J. Masters, his students and Mr. Scott Bolton, Laboratory Manager at the University of Florida. The second author would like to gratefully acknowledge funding provided by the University of Florida Alumni Fellowship.

References

[1] Simiu E, Stathopoulos T. Codification of wind loads on buildings using bluff body aerodynamics and climatological data bases. J Wind Eng Ind Aerodyn 1997;69–71:497–506.
[2] ASCE. Minimum design loads for buildings and other structures (ASCE/SEI Standard 7-05). American Society of Civil Engineers, Reston, VA; 2006.
[3] Main JA, Fritz WP. Database-assisted design for wind: concepts, software, and examples for rigid and flexible buildings. Gaithersburg (MD): National Institute of Science and Technology; 2006.
[4] NIST. "windPressure — Database-assisted-design software for rigid, gable-roofed buildings user's manual. Building and Fire Research Laboratory, Gaithersburg (MD): National Institute of Standards and Technology; 2008. Accessible at http://www.itl.nist.gov/div898/winds/homepage.htm.
[5] VORTEX-Winds. A virtual organization to reduce the toll of extreme winds on society (VORTEX-Winds). 2010. Available at https://www.vortex-winds.org.
[6] Coffman BF, Main JA, Duthinh D, Simiu E. Wind effects on low-rise metal buildings: Database-assisted design versus ASCE 7-05 standard estimates. J Struct Eng 2010;136(6):744–8.
[7] Paevere PJ, Foliente GC, Kasal B. Load-sharing and redistribution in a one-story woodframe building. J Struct Eng 2003;129(9):1275–84.
[8] Doudak G, McClure G, Smith I, Hu L, Stathopoulos T. Monitoring structural response of a wooden light-frame industrial shed building to environmental loads. J Struct Eng 2005;131(5):794–805.
[9] Zisis I, Stathopoulos T. Wind-induced cladding and structural loads on low-wood building. Journal of Structural Engineering 2009;135(4):437–47.
[10] Fischer C, Kasal B. Analysis of light-frame, low-rise buildings under simulated lateral wind loads. Wind Struct, Internat J 2009;12(2):89–101.
[11] Amini M, Kasal B. Reliability assessment of roof sheathing performance in light wood frame structures subjected to wind pressure. In: 11th world conference on timber engineering. 2010.
[12] Thampi H, Dayal V, Sarkar PP. Finite element modeling of interaction of tornado with a low-rise timber building. In: Fifth international symposium on computational wind engineering. 2010.
[13] Prevatt DO, Datin PL, Mensah AF, Martin K, Gupta R, Thang D. et al. Performance-based wind engineering of light-framed wood residential structural systems. In: 11th world conference on timber engineering. 2010.
[14] Harris HG, Sabnis GM. Structural modeling and experimental techniques. Boca Raton (FL): CRC Press; 1999.
[15] Gupta R, Miller TH, Kittel MR. Small-scale modeling of metal-plate-connected wood truss joints. J Test Eval 2005;33(3):139–49.
[16] Masters F, Gurley K, Prevatt DO. Full-scale simulation of turbulent wind-driven rain effects on fenestration and wall systems. In: 3rd international symposium on wind effects on buildings and urban environment. 2008.
[17] Vickery PJ. Component and cladding wind loads for soffits. J Struct Eng 2008; 134(5):846–53.
[18] Liu Z, Prevatt DO, Aponte-Bermudez LD, Gurley KR, Reinhold TA, Akins RE. Field measurement and wind tunnel simulation of hurricane wind loads on a single family dwelling. Eng Struct 2009;31(10):2265–74.
[19] Ho TCE, Surry D, Morrish D, Kopp GA. The UWO contribution to the NIST aerodynamic database for wind loads on low buildings: part 1. Archiving format and basic aerodynamic data. Journal of Wind Engineering and Industrial Aerodynamics 2005;93(1):1–30.
[20] Lieblein J. Efficient methods of extreme-value methodology. Washington (DC): National Bureau of Standards; 1974.
[21] Mensah AF. Determination of wind uplift forces using database-assisted design (DAD) approach for light framed wood structures, MS Thesis. Gainesville (FL): University of Florida; 2010.
[22] Stephens MA. In: D'Agostino RB, Stephens MA, editors. Tests based on EDF statistics. Goodness-of-fit techniques. New York: Marcel Dekker, Inc.; 1986.